Soft Matter

PAPER

Multiscale molecular dynamics simulations of micelles: coarse-grain for self-assembly and atomic resolution for finer details†

Pilar Brocos,[a] Paola Mendoza-Espinosa,[b] Rolando Castillo,[c] Jaime Mas-Oliva[b] and Ángel Piñeiro[*a]

A positional interpolation/extrapolation method for the mapping of coarse-grained (CG) to atomistic (AT) resolution is presented and tested for single-component micelles formed by lysophospholipids of different chain length. The target CG nanoaggregates were self-assembled from random mixtures of surfactants in explicit MARTINI water and equilibrated by molecular dynamics simulations, at the microsecond time scale. The ambiguity inherent in the definition of the CG particles was explored by mapping the same CG structures to AT resolution surfactants of different size. After the conversion, the obtained AT micelles were simulated for 250 ns and the resulting trajectories were analyzed in detail. The mean lifetime of the surfactant–solvent interactions as well as the lateral diffusion coefficients of the surfactant molecules within the micellar aggregates were obtained for the first time. The results suggest that the individual molecules within the micelle behave like lipids in a fluid membrane. The employed mapping back method is efficient and versatile, as it can be applied to diverse combinations of force fields and systems with a minimum of code development. In a general context, this work illustrates the power of multiscale molecular dynamics simulations for the generation and subsequent examination of self-assembled structures, including the fine characterization of structural and dynamic properties of the resulting aggregate.

1. Introduction

Typical micelles are relatively small self-assembled structures that form spontaneously when surfactant molecules are dissolved in water at a concentration higher than the so-called critical micelle concentration (cmc). It is well known that, in general, the average number of molecules per micelle (aggregation number), and hence its geometry/size, depends on the structure[1–3] and concentration[2,4] of the corresponding surfactant molecule as well as on the temperature,[5,6] the pH,[1,7] the ionic strength,[7] and the presence and concentration of co-solvents[8] and co-solutes.[2,9] Micelle structures have been the focus of many studies over the last century as they are of primary importance for many fundamental and technological applications.[10–14] Additionally, they represent the former structured aggregates that typically appear throughout the pathway toward the formation of more complex supramolecular structures.[15] A number of experimental techniques including surface tension, microcalorimetry, (cryo) TEM and SEM, SAXS, SANS, NMR, light scattering, sound velocity, and density measurements have been employed to characterize the structure, dynamic behavior and thermodynamic properties of micellar systems.[16,17] More recently, computational Monte Carlo (MC) and Molecular Dynamics (MD) simulation studies allowed getting complementary information at the atomic (AT) level and at the pico- and nano-second time scales. In particular, the utilization of the semi-grand-canonical ensemble in MC simulations, which keeps the number of total molecules constant but allows changing the concentration of the system by mutating the molecules identity, has recently proved to be much more efficient than the use of the canonical or grand-canonical ensembles for self-assembly studies.[18,19] The utilization of MD simulations is more popular. In some cases, AT resolution micelles can be obtained from a random mixture of surfactants in aqueous solution within a reasonable simulation time,[20–30] but most of the MD computational studies aimed at studying micelles are based on preassembled aggregates[31–38] or are performed just at the coarse-grained (CG) level.[39–46] Moreover, in some cases both approaches are combined,[47,48] adding up their respective limitations. The behavior of a preformed micelle is clearly affected by the number of surfactant molecules assigned to the structure in the simulation and, to a lesser extent, by their initial conformation. MD simulations of reverse micelles and of mixed protein–lipid systems were critically reviewed in that respect by Nevidimov and Razumov[49] and by Böckmann and

[a]Departamento de Física Aplicada, Facultad de Física, Universidad de Santiago de Compostela, Campus Vida, E-15782 Santiago de Compostela, Spain. E-mail: Angel.Pineiro@usc.es
[b]Instituto de Fisiología Celular, Universidad Nacional Autónoma de México, P.O. Box 70-243, 04510 México D.F., Mexico
[c]Instituto de Física, Universidad Nacional Autónoma de México, P.O. Box 20-364, 04510 México D.F., Mexico
† Electronic supplementary information (ESI) available. See DOI: 10.1039/c2sm25877c

Caflisch,[30] respectively. Simulations at the CG level allow one to observe the spontaneous formation of several micelles within the same simulation box from a random mixture of molecules in return for sacrificing a significant resolution level. Hybrid multiscale simulation methods, where a part of the system is represented at the AT level and the rest is considered at a lower resolution, have also been proposed.[50,51] Although these hybrid methods are expected to be well suited for protein systems, where the active site would be the best candidate for the finer representation, their role in simulations of self-assembled structures is limited to enabling the solvent or co-solvent to be modeled at a coarser level.[49] Thus, MD simulations at the CG level are proficient for self-assembly processes, while AT resolution simulations are more competent for finer studies of the resulting structures such as the interaction with the surrounding molecules, including the solvent, as well as the structure and the dynamic behavior of the molecules within the aggregate. Multiscale studies that take advantage of both resolution levels require a CG to AT mapping method. Several approaches have been developed to obtain atomistic structures from united-atom molecular representations: the so-called reverse or inverse transformations or backmapping methods.[52–56] Most of them were designed for proteins or/and lipids. They typically rely on the replacement of CG beads by groups of actual atoms selected from a pool of previously simulated systems, to perform a structural fitting based on energetic criteria. These methods are powerful but they require a reasonably large database of structures, are force field dependent, and involve significant software development effort. The first two drawbacks were recently overcome by Rzepiela et al.,[55] who presented a three-step algorithm whose central part is "a simulated annealing MD simulation in which the CG and AT structures are coupled via restraints". This procedure is effective and could be applied to any molecule, but it is relatively slow and intricate. The main aim of the present work is to propose and test a much more straightforward backmapping method based on the interpolation/extrapolation of atomic positions, taking the CG structure as a reference. The procedure is tested for single-component micelles formed by three different lysophospholipid (lyso-C_nPC) molecules of the same family: namely, 1-hexanoyl-2-hydroxy-*sn*-glycero-3-phosphocholine (HPC, CAS RN: 58445-96-8), 1-lauroyl-2-hydroxy-*sn*-glycero-3-phosphocholine (LPC, CAS RN: 20559-18-6), and 1-palmitoyl-2-hydroxy-*sn*-glycero-3-phosphocholine (PPC, CAS RN: 17364-16-8). The three-dimensional structure of LPC at the atomic level is illustrated in Fig. 1 (right). The choice of compounds from a homologous series had a double goal: (i) to analyze the influence of the acyl-chain length on the micelle features; and (ii) to explore the ambiguity inherent in the definition of the CG beads by mapping back the same CG structures into two different AT molecules. The motivation of selecting that particular zwitterionic family was to reproduce a model system (lyso-C_{12}PC micelles) used in previous experimental studies by some of us[57] to mimic the surface of high density lipoproteins. Our attempts to get well-defined lyso-C_nPC micelles at atomic resolution and affordable time scales by spontaneous self-assembly failed, in contrast to the success experienced with other surfactants,[26] so requiring the use of more powerful simulation methods such as that introduced in the present work. Henceforth, the paper is organized as follows:

first, the simulation methodology for the coarse-grained and atomistic resolution levels, as well as the mapping back approach, is described in detail. Second, the main results for both types of simulations are examined, including for the finer study the structure and dynamic behavior of surfactants within the aggregates and micelle–solvent interactions. Finally the main conclusions are briefly discussed, stressing the multiscale simulation methods' suitability to deal with nanoaggregates and analyzing how the strengths of each resolution level are exploited in such context.

2. Methodology

2.1. General simulation parameters

Simulations at both CG and AT resolution levels were performed using periodic boundary conditions with the GROMACS MD engine version 3.3.3.[58,59] The initial velocities were randomly assigned to produce a Maxwell distribution at the working temperature. The equations of motion were integrated using the leapfrog method with 30 fs and 2 fs time steps for the CG and AT simulations, respectively. All the simulations were performed in the NPT ensemble. Water and surfactant molecules were separately coupled to a Berendsen thermostat[60] at 300 K with a common period of 1 ps (CG) and 0.1 ps (AT). The pressure was isotropically controlled at 1 bar using a Berendsen barostat[60] with an isothermal compressibility of 5×10^{-5} bar^{-1} (CG) and 4.6×10^{-5} bar^{-1} (AT). The analysis of the trajectories was performed using tools of the GROMACS package, the viewers RasMol 2.7 and PyMOL 0.99,[61,62] as well as programs specifically developed for this work. Detailed descriptions of each simulation type as well as of the CG to AT transformation method are given below.

2.2. Coarse-grained simulations

The MARTINI force field (version 2.0) developed by Marrink et al.[63] was employed to model all the CG molecules. This force field is based on a four-to-one mapping, meaning that on an average four heavy atoms are represented by a bead or single interaction center. As proposed for phosphatidylcholine (PC) lipids,[63] the lyso-C_nPCs were parameterized using four beads for the PC head together with the first 2–3 CH_2 groups of the surfactant tail, and one, two or three additional hydrophobic beads (HB) for the rest of the tail. Unless the coarse-graining procedure is set up to be close to the chemical structure,[52] the loss of resolution inherent to CG force fields introduces ambiguities in the definition of the molecules, in such a way that several AT structures could be modeled using the same CG representation. Thus, we decided to refer to these CG structures as nHB-PC (with $n = 1$, 2 or 3 indicating the number of HBs) instead of using names of real molecules. Random mixtures consisting of 234 CG molecules and ~23 000 MARTINI water particles were introduced in rhombic dodecahedron boxes of edge length 15 nm. Bearing in mind that the solvent is also affected by the four-to-one mapping, the total concentration of surfactant molecules in the simulated systems is ~139 mM. This should suffice to produce aggregates even in the 1HB-PC case, as the MARTINI force field has been reported to underestimate the cmc of zwitterionic and nonionic surfactants by two orders of magnitude at

298 K[45] (the cmc of PPC and LPC are 0.007 and 0.7 mM, respectively, whereas that of HPC is estimated to be around 700 mM by extrapolation[64]). Each system was energy minimized using the steepest descent method and then six independent 5 µs long trajectories per system were performed starting from different initial random velocities. A cutoff of 1.2 nm was employed for the nonbonded interactions. The L–J potential was smoothly shifted to zero between 0.9 and 1.2 nm. A similar approach was employed for the electrostatic interactions, considering a Coulombic potential with a relative permittivity of 15 together with a shift function from 0 to 1.2 nm. The neighbor list was updated every 10 steps.

2.3.   Atomistic simulations

The AT simulations were performed using the extended simple point charge (SPC/E) water model together with the GRO-MOS96 (53a6) force field for the surfactant molecules. The parameters for the bonded interactions of the lysophospholipids were adapted from the Berger[65] based topologies for members of the 1,2-diacyl-sn-glycero-3-phosphocholine family, available at the Tieleman's lab webpage.[66] In order to build the AT simulation boxes, selected CG micelles were backmapped (see next subsection) and introduced in rhombic dodecahedron boxes of such dimensions so as to leave a minimum distance of 0.8 nm from the walls to any micelle atom. The simulation box was then filled with a number of water molecules ranging from 10 452 to 13 063, depending on the system. After energy minimization, the systems were simulated for 250 ns with the configurations stored every 10 ps for analysis. Nonbonded interactions were evaluated using a twin range cutoff of 0.8 and 1.4 nm. Interactions within the shorter and longer cutoffs were updated every step and every five steps, respectively. Beyond the 1.4 cutoff, a reaction field correction was applied with a relative permittivity of 78. The use of a reaction field instead of the more accurate PME algorithm for the evaluation of the long range interactions was chosen to save computational time, assuming that the influence of that choice is small in the simulation of our target systems: relatively compact micelles. Note that the use of PME would slow down the simulations by a factor of ∼3 and that its effect is expected to be more serious for the simulation of self-assembly processes, not considered at the AT level in the present work. The bond lengths and H–O–H angle in water were constrained using the SETTLE algorithm; the LINCS algorithm was used to constrain bond lengths in the surfactant molecules.

2.4.   Description of the backmapping method

A representative micelle for each CG molecule was selected from the several nanoaggregates spontaneously built throughout the CG trajectories (see below). The atomic coordinates of each surfactant molecule forming the micelle were obtained by simple geometrical interpolation/extrapolation of the CG coordinates, approximating the distances and angles between bonded atoms. More specifically, the AT representation of a linear chain, where each CG bead is transformed into n atoms, is obtained by using the position of the reference CG particle for the first atom and distributing the remaining $n - 1$ coordinates along the segment joining two consecutive CG particles, at equivalent distances
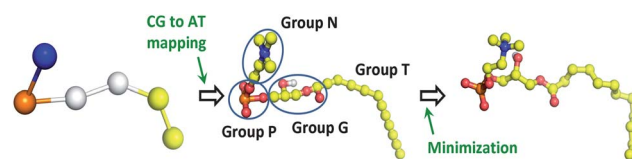

Fig. 1 Illustration of the backmapping methodology for the transformation of a single CG 2HB-PC structure (left) to a minimized AT LPC molecule (right). The direct result from the interpolation/extrapolation method applied to the CG structure before minimization is also shown (center). This intermediate conformation is used to define the four atomic groups (N, P, G, and T) employed for the subsequent analysis of the interactions with solvent molecules. Yellow spheres represent the two hydrophobic beads in the CG structure and the carbon atoms in the AT structures, where the following color assignments were also made: blue for nitrogen, red for oxygen, orange for phosphorus, and white for polar hydrogen.

from each other. To map a terminal group into several atoms, the new $n - 1$ coordinates are obtained by extrapolation in the opposite direction of the vector joining the terminal CG particle with the preceding one. Any extrapolation was performed by using a conservative approach to the bonding distance between the corresponding atoms to avoid overlapping with neighbor molecules after the backmapping process. The peripheral atoms in a chain were placed with a random orientation on the plane containing their corresponding reference bead and perpendicular to the segment that connects such a bead with the closest one. In order to examine the ambiguity in the definition of the MARTINI particles,[67] each of the hydrophobic beads of 2HB-PC (3HB-PC) was mapped back into 2 (3) or $4\frac{1}{2}$ ($4\frac{1}{3}$) CH_2 groups on average. Thus, a total of five AT micelles were obtained from the backmapping of the three selected CG nHB-PC micelles. A minimization of the system using the AT force field was performed after the backmapping process in order to optimize the structure of the molecules as well as their interaction with neighbors. In the present work the GROMOS96 G53a6 force field with the GROMACS software was employed with such purpose, but it is worth noting that the procedure would be equivalent to any other combination of force field and MD engine. The whole process for the transformation of a single CG 2HB-PC structure to an AT LPC molecule, which takes just a few seconds in a standard computer (thus affording a typical micelle of tens of units in ∼1 minute), is illustrated in Fig. 1.

3.   Results and discussion

3.1.   Coarse-grained MD simulations and selection of the CG micelles

As explained above, six 5 µs long MD simulations were performed for each of the three nHB-PC structures (n = 1, 2, 3), starting in each case from 234 CG solute molecules at random positions/orientations that were dissolved in ∼23 000 CG water particles. The spontaneous aggregation of the nHB-PC units within each simulation box was monitored as a function of time by using cutoff values of 0.4, 0.5, 0.6, and 0.7 nm to define the direct interaction between them. It was found that 0.4 nm is too short to study the molecular contact at this resolution level (which is not surprising as 0.47 nm is the closest distance of approach between two particles[63]) while the results obtained
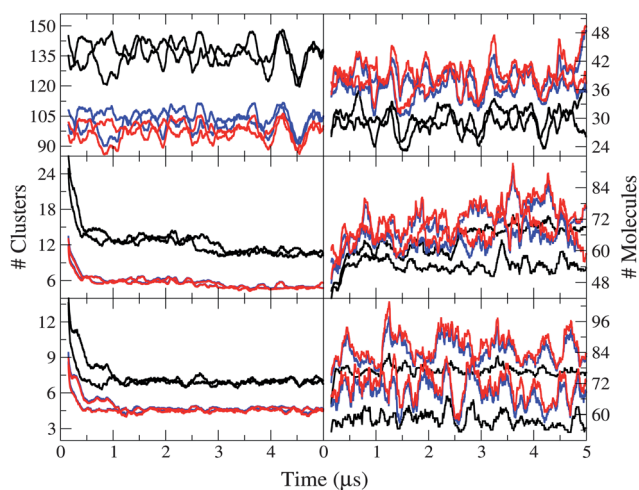
Fig. 2 Number of clusters (left) and number of molecules of the largest one (right) as a function of time, for two of the six trajectories run for 1HB-PC (top), 2HB-PC (middle) and 3HB-PC (bottom). The analysis was performed by using three different cutoffs to define the interaction between CG molecules, namely 0.5 (black), 0.6 (blue) and 0.7 nm (red). Data were progressively averaged over 3 ns for clarity. Note that in the middle-left and bottom-left panels the blue and red curves are indistinguishable.

using 0.6 and 0.7 nm are similar, as shown in Fig. 2 for two representative trajectories of each system. For comparison, Sanders and Panagiotopoulos[45] and Kraft et al.[67] selected by visual inspection a cutoff of 0.6 nm to trace the cluster behavior of dodecylphosphocholine and 1,2-dihexanoyl-sn-glycero-3-phosphocholine, respectively, under the MARTINI force field. It also appears from Fig. 2 that the selected time scale, which is hardly reachable at atomistic resolution for systems of similar size, is appropriate for this kind of self-aggregation studies. The expected trend, namely, that the number of clusters decreases throughout the trajectories as their size grows, is exemplified by the 2HB-PC case (Fig. 2, middle). A much faster initial decrease in the number of 3HB-PC clusters leads to finished growth of the largest aggregates at the very beginning of the trajectory (right

panel at the bottom). In the 1HB-PC case, the number of clusters suffers large fluctuations but no drift, thus revealing a pre-cmc state. The larger the number of hydrophobic beads in the CG molecule, the lower the number of clusters and the larger the maximum number of units forming the aggregates. Considering the information obtained from this analysis, three micelles consisting of 33, 67, and 84 nHB-PC with $n = 1$, 2, and 3, respectively, were chosen for the backmapping process and subsequent AT MD simulations. The selected aggregates were those with the largest number of molecules that were shown to be stable for a significant part of the trajectory. They are expected to be well suited to later study macromolecule–micelle interactions, which is of interest to us to complement previous experiments.[57] Note that the fluctuations in the right panel of Fig. 2, indicating the number of nHB-PC units in the largest aggregate, are due to collisions (approximations within the cutoff) between CG particle clusters throughout the trajectories. For the larger cutoffs (0.6, 0.7) such events may be also revealed by a fractional average number of clusters in the stationary part of the trajectory (Fig. 2, left panel at the bottom). As stated in the Methodology section, all the CG simulations presented in this work were performed using the standard MARTINI water model as solvent. The employment of the polarizable MARTINI water[68] (PLW) instead has very recently proven to reproduce better the micellization properties of 1,2-dihexanoyl-sn-glycero-3-phosphocholine in MD simulations at CG resolution, by increasing the concentration of free surfactant and decreasing the average size of the aggregates.[67] The use of PLW in our systems does not have any practical advantage since the simulations would be ~3 times slower and we are not aiming to simulate real molecules at the CG level, but nHB-PC structures that will later be mapped to different real AT molecules.

3.2. Backmapping of the CG aggregates and atomistic MD simulations

The backmapping process was performed as explained in the Methodology section. Thus, five AT micelles were obtained from the three selected CG aggregates (Fig. 3), namely, two HPC
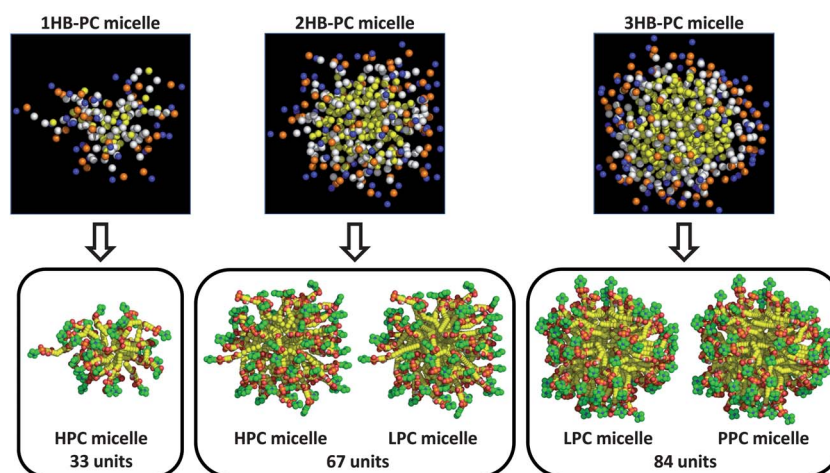

Fig. 3 Transformation of the three selected CG aggregates into five AT resolution structures. The molecule type and number of units per structure are indicated next to each image. The color assignments are those of Fig. 1 except for carbon atoms in the choline group, which are colored green for the sake of clarity.
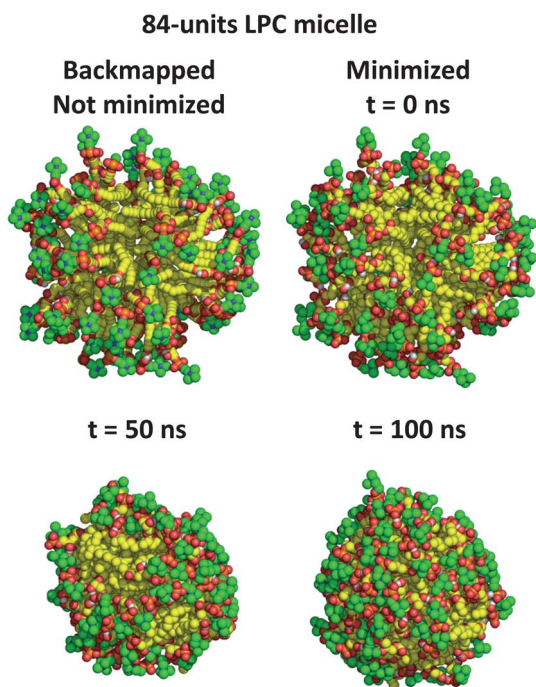
84-units LPC micelle

Backmapped Not minimized   **Minimized t = 0 ns**

t = 50 ns   **t = 100 ns**

Fig. 4 Evolution of an 84-LPC micelle from the just backmapped structure up to 100 ns. No evident structural differences were observed after 50 ns. Same color assignments as in Fig. 3.

micelles with 33 and 67 molecules, two LPC micelles with 67 and 84 molecules and one PPC micelle with 84 molecules. 250 ns long trajectories were run for each of the five AT systems and the structural changes and dynamic behavior of the surfactant molecules and their aggregates were assessed. Typically, the aggregates experience a quick packing enhancement during the first ns of the AT trajectory (Fig. 4). This is probably due to the use of equal-sized spherical beads in the MARTINI CG force field[63] that, although could be well suited for the simulation of nearly flat structures, like lipid bilayers, are less suitable for highly curved nanoaggregates like micelles. In the literature, the use of different-sized beads to account for the micelle curvature has been proposed in the context of a coarser level of coarse-grained molecular dynamics.[47] Another coarse-graining strategy intended to mimic the biomembrane bending was successfully tested with a member of the 1,2-diacyl-sn-glycero-3-phosphocholine family, by modeling the choline and phosphate moieties with two spherical beads and the glycerol-ester and hydrocarbon regions with chains of ellipsoids.[69]

Both the compacting stage and the optimization of the micelle structure after the backmapping process are reflected in the time evolution of several dynamic and structural properties of the surfactants as well as in their interaction with the solvent molecules.

3.3. Properties of the micelles

3.3.1. Volume per surfactant. The average volume available per surfactant molecule (V_s) as a function of time was determined by:

$$V_s = (V_t - V_w)/n_s \qquad (1)$$

where V_t is the total volume of the simulation box, V_w is the expected volume for the number of water molecules in the system if they were isolated at identical temperature and pressure, and n_s is the number of micellized molecules. Although the initial V_s values were relatively high (0.60 and 0.67 nm^3 for the 33- and 67-HPC systems, 0.73 and 0.79 nm^3 for the 67- and 84-LPC systems and 0.85 nm^3 for the 84-PPC micelle), they reached significantly lower values within a few hundred ps, then remaining stable until the end of the trajectories (Table 1 and Fig. S1†). The aggregation number barely affects the volume available for each molecule, but the effect of changing the lyso-C$_n$PC chain length is evident. The volume corresponding to each CH$_2$ group in the micelles can be easily obtained from the differences $V_{LPC} - V_{HPC}$ and $V_{PPC} - V_{LPC}$, affording 26.89 and 27.04 Å^3, respectively. This result is in agreement with those reported for PC lipid bilayers by Uhríková et al.[70] (27.52 Å^3 at 298 K) and by Nagle and Tristram-Nagle[71] (25.9 Å^3 at 293 K and 28.3 Å^3 at 303 K).

3.3.2. Solvent-accessible surface. The solvent-accessible surface (SAS) area per molecule showed to be much more sensitive to the number of surfactant molecules in the micelle. Again, its values are unrealistically large at the beginning of the simulation but, in contrast to V_s, it takes between 10 and 25 ns to achieve a stable value. In the literature, the stabilization time for this magnitude in pre-built micelles goes typically from 1 to 15 ns.[22,32,34,37,38] The SAS area per molecule in the 33-HPC micelle is almost the same as in the 67-LPC micelle, while it is significantly lower in the case of the 67-HPC micelle and to a lesser extent in the system with 84 LPC units (Fig. 5 and Table 1). This can be summarized in the empirical finding of a linear correlation between the SAS area per surfactant and the n/n_s ratio, with n standing for the number of carbon atoms in the tail group (see Fig. S2†). Such a trend is mainly caused by the hydrophobic SAS,

Table 1 Average volume (V_s) and solvent-accessible surface (SAS) area per surfactant molecule, average distance from the N or P atoms to the center of mass of the micelle, and average cosine of the angle formed by the atoms P and N and the center of mass of the micelle, for the 5 systems simulated at the atomistic level

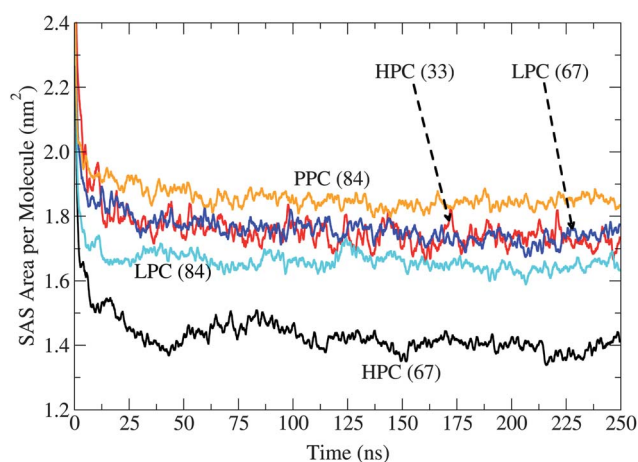| | V_s (nm^3) | SAS area (nm^2) | Average distance (nm) | | Average cosine of P–N–c.o.m. angle |
			N–c.o.m.	P–c.o.m.	
HPC (33)	0.503 ± 0.017	1.741 ± 0.050	1.45 ± 0.24	1.35 ± 0.20	0.38 ± 0.28
HPC (67)	0.4926 ± 0.0088	1.416 ± 0.042	1.82 ± 0.27	1.73 ± 0.23	0.38 ± 0.25
LPC (67)	0.6596 ± 0.0089	1.749 ± 0.042	2.08 ± 0.23	1.99 ± 0.19	0.34 ± 0.24
LPC (84)	0.6591 ± 0.0077	1.655 ± 0.036	2.24 ± 0.25	2.15 ± 0.21	0.32 ± 0.23
PPC (84)	0.7673 ± 0.0078	1.846 ± 0.036	2.36 ± 0.25	2.27 ± 0.21	0.35 ± 0.25

Fig. 5 Solvent-accessible surface area per molecule as a function of time for the five AT simulations indicated in the plot. Data were progressively averaged over 0.5 ns for clarity.

despite this contribution representing a modest percentage of the total SAS (between 27 and 41%, as shown in Table S1†). Yoshii and Okazaki,[33] who studied the variation of the average SAS area in a series of growing sodium dodecyl sulfate micelles, also observed that its hydrophobic contribution suffers a more marked decrease with increasing n_s than the hydrophilic one. In that specific instance, the hydrophobic SAS would be "a result of *gauche* defects introduced in the chain due to packing constraints near the center of the micelle", according to Shang *et al.*[34] The interpretation in the case of lyso-C_nPC micelles is not that straightforward, because the hydrophobic SAS is not only composed of solvent-accessible segments from the hydrocarbon region. The force field parameterization of these molecules assigns negligible partial charge to both the N atom and the terminal CH_2 at the choline moiety, and the two CH_2 at the glycerol-ester moiety; hence they are treated as hydrophobic elements too.

3.3.3. Size and geometry. The distance of every N and P surfactant atom to the center of mass (c.o.m.) of the corresponding aggregate was determined to assess its size and dynamic deformation as a function of time (Fig. 6). The average of these values over all the molecules and frames could be interpreted as a measurement of the micelle geometrical radius. As expected, the results indicate that the larger the surfactant and the aggregation number, the bigger the micelle (Table 1). Moreover, the obtained aggregates are not rigid. The surfactants diffuse laterally over their surface and also move in and out along the radial direction, as illustrated in Fig. 6. The relatively large uncertainties in the N/P–c.o.m. distances (Table 1) result from these latter fluctuations. However, the N and P atoms of the surfactant molecules typically spend more time at the average distance from the c.o.m. than at any other distance, as illustrated by the normal distributions obtained from the corresponding data (Fig. S3†). This suggests a spherical geometry, agreeing with our visual inspection and with the analysis of PGSTE-NMR measurements made by Vitiello *et al.*[72] The distance distributions are sharper for the P atoms than for the N atoms, which is consistent with the P–c.o.m. distances being slightly shorter in average, hence
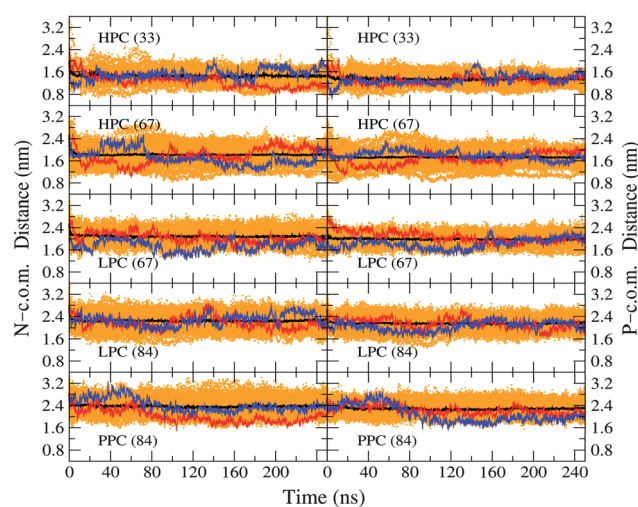

Fig. 6 Distance from each N (left) or P (right) surfactant atom to the center of mass of the corresponding micelle (orange spots) together with the average value for each frame (black curve) as a function of time. The red and blue curves are intended to illustrate the mobility of the lyso-C_nPC molecules within the aggregate and correspond to the distances from two randomly selected N (left) or P (right) atoms to the c.o.m. of the corresponding micelle. The type and number of surfactant molecules of the system are indicated in each panel.

making the P atoms more hindered than the N atoms. The average N–c.o.m. distance can be understood as the hypothetical radius of a hard sphere with the same mass and density as the studied micelle and is expected to be closely correlated to the (larger) hydrodynamic radius, which includes solvent and shape effects.[73–75] The comparison between both quantities is made in Table S2,† where the hydrodynamic radii were collected from the literature.[57,72,76] As a kind of consistency test, Fig. S2† shows that there is a good linear correlation between the SAS and hard-sphere areas per surfactant. The standard deviation of the straight line increases significantly when the P–c.o.m. distance is taken as the geometrical radius instead of N–c.o.m., despite the corresponding distribution being narrower. The geometry of the aggregates was also assessed by measuring their principal moment of inertia (Fig. S4†) to confirm that all the simulated micelles are nearly spherical.

3.3.4. Order of the aliphatic tails. The internal order of the aliphatic tails in micelles was estimated by defining the local order parameters as:

$$S_i = (3\cos\theta - 1)0.5 \qquad (2)$$

where θ is the angle between the vectors connecting carbon atoms ($i - 1$, $i + 1$) and (i, $i + 2$) in the surfactant tail. This allows quantifying deviations from *trans* conformations of hydrocarbon chains regardless of the molecule orientation. As in the case of V_s, this structural property does not seem to be highly sensitive to the micelle size, for a given lyso-C_nPC. The average S_i values for each C–C–C–C group of atoms at several simulation frames, including the initial conformation obtained just after the minimization of the system, are very similar to each other, typically ranging from 0.8 to 0.9 (then the average θ going from 30 to 21°).
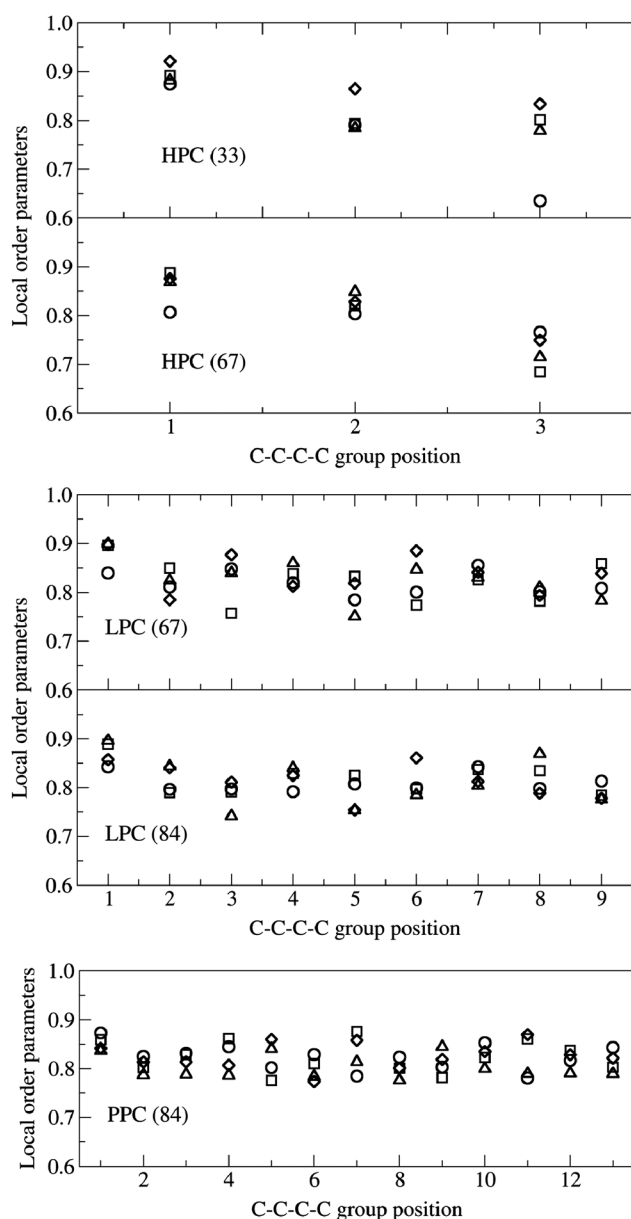
Fig. 7 Average local order parameters (eqn (2)) over the hydrocarbon chain of the surfactant molecules for the systems indicated in the plots and for the structures corresponding to 0 ns (○), 1 ns (□), 5 ns (Δ) and 250 ns (◇) of each trajectory.

The S_i values obtained for the different surfactants are also quite similar although their dispersion seems to decrease as the length of the lyso-C_nPC tail increases (Fig. 7). Thus, only for the simulations with HPC some S_i values corresponding to the terminal C–C–C–C group are lower than 0.7, while the PPC tails exhibit the lowest amount of *gauche* defaults throughout the entire chain and trajectory.

3.3.5. Orientation of the head groups.
To further explore the structure of the surfactants within the micelles, the P–N–c.o.m. angle formed by the segment joining the P and N atoms and that connecting the N atom with the c.o.m. of the aggregate was also measured as a function of time for each molecule (Fig. S5†). This

is mostly a measurement of the N–P orientation with respect to the micelle radius. It was found that practically all the acute angles were reachable, although with different probability (Fig. S3†). As a result, the average cosine values exhibit a large uncertainty of ~70% (Table 1). The angle distribution mode is asymmetrical and shifted toward low cosine values, indicating that the most frequent angle is close to 90° for all the simulations (Fig. S3†). The distribution corresponding to the smaller aggregate – that gathering 33 HPC molecules – appears to be bimodal, exhibiting a second small maximum at cos(P–N–c.o.m.) close to 0.9. This is added evidence of some disorder in the molecules of that specific aggregate. Note also that the angle distribution mode for the 67-HPC micelle is borderline between unimodal and bimodal.

3.3.6. Surfactant lateral diffusion within micelles.
The lateral diffusion of the surfactant molecules across each micelle, *i.e.* the diffusion over the surface of the aggregates, was estimated from the two-dimensional displacement distributions over specific time intervals (Δt). The employed methodology was identical to that recently described by Niemelä *et al.*,[77] but instead of considering lateral displacements in a plane the attention was fixed on the average length of the path followed by the N or P atom of the surfactant molecules over the micelle surface. As expected, the larger the time employed to determine the displacements the wider the distributions (Fig. 8 and S6†). The lateral diffusion coefficients obtained for 6 different Δt intervals do not exhibit a significant dependence on the surfactant size or on the number of molecules in the aggregate (Fig. S7†), but their degree of time-dependence decreases with increasing micelle radius. Their values (~4 to 12×10^{-7} and 7 to 9×10^{-7} $cm^2 s^{-1}$ for the smallest and the biggest aggregate, respectively) are similar to those typically found at the upper range for lipids in fluid bilayers.[77–79] Interestingly, the experimental intradiffusion coefficient of LPC micelles well above the cmc is 7×10^{-7} $cm^2 s^{-1}$,[72] which means that the diffusivity of a surfactant molecule in
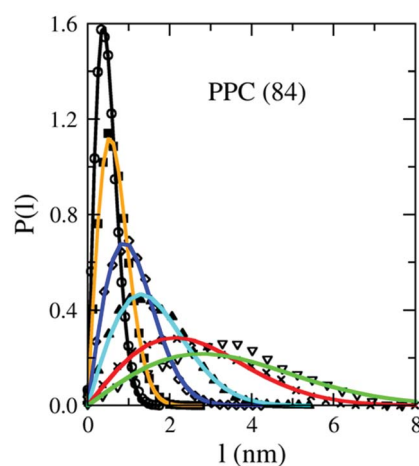

Fig. 8 Distribution of the lateral displacements (*l*) of the P atoms over the surface of the 84-PPC micelle for 6 different Δt values. Data were fitted to the expected two-dimensional random-walk distribution as detailed by Niemelä *et al.*[77] (see eqn (3) in the ESI of the referenced work) to obtain the lateral diffusion coefficients displayed in Fig. S7.† Symbols (dot type, curve color): 1 ns (○, black), 2 ns (■, orange), 5 ns (◇, blue), 10 ns (▲, cyan), 25 ns (x, red), and 50 ns (∇, green).

Table 2 Average number of water molecules at less than 4 Å from any atom of groups G, N, P, and T, as defined in Fig. 1

	G	N	P	T
HPC (33)	10.34 ± 0.38	7.04 ± 0.34	3.39 ± 0.18	2.31 ± 0.27
HPC (67)	8.08 ± 0.22	6.42 ± 0.20	3.15 ± 0.13	0.85 ± 0.15
LPC (67)	9.28 ± 0.24	6.68 ± 0.24	3.33 ± 0.15	0.92 ± 0.13
LPC (84)	8.64 ± 0.22	6.44 ± 0.21	3.26 ± 0.11	0.77 ± 0.10
PPC (84)	9.36 ± 0.22	6.41 ± 0.20	3.24 ± 0.12	0.91 ± 0.12

the micelle and that of a micelle in the solvent are comparable processes in aqueous solutions of LPC. Since the two-dimensional displacements employed to generate the distributions are the product of the micelle radius (average of either the N–c.o.m. or P–c.o.m. distances) by the swept angle at different time intervals, their values are bound. This is reflected in the shape of the distributions for the largest Δt values and in their poor fitting to the two-dimensional random-walk function, as well as in the decreasing diffusion coefficients obtained from them (Fig. S7†).

3.3.7. Hydration. The interaction of solvent molecules with the micellized surfactants was assessed in detail. For this analysis the lyso-C_nPCs were divided into four atomic groups (see Fig. 1) and the total number of waters at less than 4 Å from any atom of a given group was averaged over the surfactant molecules forming each micelle. Fig. S8† and Table 2 show that these hydration numbers seem to be more sensitive to n_s than to n. Also, increasing n_s gives rise to lower dispersion in the average number of waters contacting a given group, after the first few (10–25) ns of the transitory regime. The four groups are significantly more hydrated in the 33-HPC aggregate than in the rest of the micelles, including that formed by 67 HPC molecules. The difference between the micelles with 67 and 84 LPC molecules is also clear, with significantly less hydration for the latter. In contrast, the little differences found in the hydration levels of the 67-LPC and 84-PPC aggregates suggest that larger micelles could be formed with PPC molecules. This is consistent with the finding at 308 K of a concentration-independent PPC aggregation number of 139, by using static light scattering.[80] Also, the extrapolation of data reported by Vitiello et al.[72] for four shorter members of the lyso-C_nPC family at 298 K would afford for PPC in D_2O an aggregation number of 115. The N group has more water molecules within its (4 Å)-shell than the P group, as expected from the comparison of the N–c.o.m. and P–c.o.m. distances (Table 1). Outstandingly, in all the cases the G group is, by far, the most exposed to the solvent despite its central position in the lyso-C_nPC molecules. The direct visualization of the systems with a molecular viewer suggests that this paradoxical effect is due to the inability of trimethylammonium to participate in a hydrogen bond[81] together with the capability of the glycerol-ester moiety of being both a hydrogen bond donor and an acceptor. Anyway, this result is in good agreement with that obtained by Vitiello et al.,[72] who described the lyso-C_nPC micelles as presenting a thick external layer constituted by highly hydrated glycerophosphatidylcholine groups and identified the glycerol-ester moiety as being partly responsible for this feature.

3.3.8. Mean lifetime of the surfactant–solvent interactions. The dynamic behavior of waters was also monitored to assess the
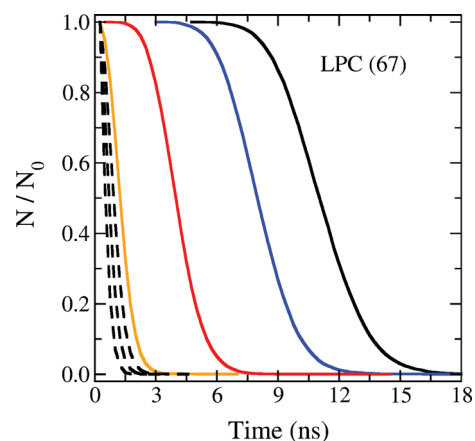

Fig. 9 Decay functions in the 67-LPC micelle for the normalized water–surfactant contact number, N/N_0, intended to illustrate the time the interactions stand. Contacts are defined by using a cutoff of 4 Å. The number of contacts for a given group at the starting point (50 ns of MD simulation), N_0, is used as normalizing constant and taken as reference to follow their lifetime through the variable N. The calculations were performed for the last 200 ns of the atomistic trajectories and for the atomic groups G (solid black), N (blue), P (red), and T (orange), as defined in Fig. 1. Dashed black curves stand for the sequential deletion in T group of the C-atom pairs that are closest to the surfactant polar head and show the corresponding decrease in the mean lifetime of the interaction.

mean lifetime of their interaction with the different atomic groups of the surfactant molecules in the micelle. The decay functions of such interactions (Fig. 9 and S9†) are normalized by the corresponding number of contacts at the starting time in this analysis (50 ns in all cases) and so they give an idea of the interaction lifetime regardless of the solvation level of each surfactant region. The mean lifetime can be approached as the time at which the ordinate in the decay functions (N/N_0) equals e^{-1} (see Table 3).[82] Our results clearly show that the stability of the interactions of water molecules with the different atomic groups decreases in the following order: G > N > P > T; and still decreases when examining segments of the surfactant chain that are farther from the polar head (see columns T-2, T-4 and T-6 in Table 3). This calculation, based on the dynamics of solvent molecules, seems to be more sensitive to the length of the surfactant molecule than the results obtained from the previous water analysis. The stability of the interactions with the G group shows a clear evolution with the size of the surfactant, and it seems to be highly sensitive to the number of micellized molecules too. In contrast with other properties, the mean lifetime of the

Table 3 Mean lifetime of the water–surfactant contacts for the G, N, P, and T groups (values expressed in ns), calculated as the time at which the decay function (Fig. S9†) equals e^{-1}. The columns labeled as $T - m$ represent the T group, as defined in Fig. 1, with the removal of the first m C-atoms, starting from the polar head

	G	N	P	T	T − 2	T − 4	T − 6
HPC (33)	7.24	4.99	2.50	1.96	1.47	0.99	
HPC (67)	10.49	8.23	4.23	1.47	1.21	0.94	
LPC (67)	11.75	8.73	4.48	1.49	1.21	0.95	0.70
LPC (84)	12.00	9.23	4.74	1.46	0.99	0.75	0.69
PPC (84)	12.99	9.00	4.74	1.71	1.22	0.96	0.70

interactions increases when n_s increases. It is also worth noting that the differences found among the studied systems in the lifetime of the interaction of water molecules with the surfactant tails are relatively low when compared to what happens with group G and, to a lesser extent, with group N. This explains the lack of penetration of water molecules in the core of the micelles and suggests that the observed contacts in this region result from the surfactant dynamics rather than from the existence of entrapped waters.

4. Conclusions

By using multiscale MD simulation, a new strategy for the study of micelle-like nanoaggregates has been proposed. The method takes advantage of the large time scales accessible at the coarse-grained level, allowing the self-assembly stage to be efficiently completed. Afterwards, it makes use of a quick and straightforward technique based on geometrical interpolations/extrapolations to map the aggregates back to the atomistic level. It is undoubtedly useful when well-defined micelles are not reachable with AT resolution at affordable time scales. This allows further studies of more complex systems like complexes formed by structured molecular aggregates and macromolecules. The procedure is also expected to be well suited for dealing with lipid membranes, taking into account that the employed CG force field was parameterized for lipids in origin.[63] In contrast to the reported mapping back techniques that are force field dependent, the one presented here could be applied to any combination of CG and AT force fields and with any MD engine, because it lies on simple geometrical rules.[83] In fact, a CG model using ellipsoidal beans for the surfactant tail[69] would probably work better in the present case (by reducing the time needed to attain the stationary state in the atomistic simulations), as the self-assembly would account for the high curvature of micelles more faithfully. The interpolation/extrapolation process could be refined to deal with proteins or DNA. Nevertheless, optimization would probably be worthless in the present case since the employed CG force field appears to be a more serious limitation for the study of micelles than the mapping back method. Note that the main aim of the present work is in no way to assess any CG or AT force field or parameterization of the employed molecules, but to test the combination of two resolution levels by mapping the system from low to high resolution. Another useful feature of the proposed micelle generation method is the possibility of selecting aggregates of the desired size amongst the array obtained from one or several CG self-assembly simulations. Thus, in the case of lysophospholipid micelles, which are typically used as biomembrane mimics[72] in studies of membrane interaction with peptides, our obvious choice pointed to the right side end of the size distributions.

A complete and detailed analysis of the structure and dynamics of lyso-C_nPC micelles ($n = 6, 12, 16$) was performed at the atomic level. The ambiguity inherent to the correspondence between coarse- and fine-grained descriptions was explored in the case of the CG MARTINI force field, taking advantage of it to compare micelles that only differ from each other either in the number of surfactants (n_s) or in their hydrocarbon chain length. This led to the empirical finding of a linear correlation between the SAS area per surfactant and the n/n_s ratio that is mainly governed by the hydrophobic SAS. At the opposite end, the

molecular volume of micellized lyso-C_nPCs seems to be a quantity insensitive to n_s changes for these systems. The analysis of the atomistic trajectories has also been helpful to identify which properties are the most appropriate to recognize the attainment of the stationary state (SAS area and hydration number) and which ones are the best suited to detect order differences between systems (order of the aliphatic tails and orientation of the head groups). The lateral diffusion of surfactants within micelles was determined for the first time, indicating that the individual molecules diffuse in the micelle as lipids do in fluid membranes. Additionally, the mean-lifetime of the interaction between the solvent and the surfactant molecules was also determined for different molecular groups. The latter analysis indicates that no water molecules are trapped in the micelle core and that the short lifetime interactions of the solvent with the surfactant tails are due to the movement of the micelle components in the radial direction within the aggregate. In addition to the implementation of a methodology to efficiently study molecular aggregates at the atomic level, this work also provides new insight that contributes to the better understanding of micellar aggregates.

Acknowledgements

References

1 A. H. E. Müller, Y. Cai, M. Hartenstein, M. Gradzielski, M. Zhang, H. Mori and D. V. Pergushov, *Polym. Prepr. (Am. Chem. Soc., Div. Polym. Chem.)*, 2004, **45**, 267–268.
2 X.-X. Meng and W. B. Russel, *Macromolecules*, 2005, **38**, 593–600.
3 S. Chavda, P. Bahadur and V. Aswal, *J. Surfactants Deterg.*, 2011, **14**, 353–362.
4 S. Hait, P. Majhi, A. Blume and S. Moulik, *J. Phys. Chem. B*, 2003, **107**, 3650–3658.
5 I. Goldmints, F. von Gottberg, K. Smith and T. Hatton, *Langmuir*, 1997, **13**, 3659–3664.
6 E. Karayianni, R. Jérôme and S. Cooper, *Macromolecules*, 2000, **33**, 6473–6484.
7 M. Burkhardt, N. Martinez-Castro, S. Tea, M. Drechsler, I. Babin, I. Grishagin, R. Schweins, D. Pergushov, M. Gradzielski, A. Zezin and A. Müller, *Langmuir*, 2007, **23**, 12864–12874.
8 G. Colafemmina, D. Fiorentino, A. Ceglie, E. Carretti, E. Fratini, L. Dei, P. Baglioni and G. Palazzo, *J. Phys. Chem. B*, 2007, **111**, 7184–7193.
9 J. Singh, J. Miller and R. Ranganathan, *J. Phys. Chem. B*, 2007, **111**, 9317–9324.
10 H. Nishi, *J. Chromatogr., A*, 1997, **780**, 243–264.
11 G. Gaucher, M. Dufresne, V. Sant, N. Kang, D. Maysinger and J. Leroux, *J. Controlled Release*, 2005, **109**, 169–188.
12 V. Torchilin, *Pharm. Res.*, 2007, **24**, 1–16.
13 R. O'Reilly, *Philos. Trans. R. Soc., A*, 2007, **365**, 2863–2878.
14 Y. Liu, X. Dong and Y. Sun, *Chin. J. Chem. Eng.*, 2008, **16**, 949–955.
15 A. Blanazs, S. Armes and A. Ryan, *Macromol. Rapid Commun.*, 2009, **30**, 267–277.

16 S. Croy and G. Kwon, *Curr. Pharm. Des.*, 2006, **12**, 4669–4684.
17 G. Riess, in *Handbook of Industrial Water Soluble Polymers*, ed. P. A. Williams, Blackwell Pub., Oxford, 2007, ch. 7.
18 P. G. Bolhuis and D. Frenkel, *Phys. A*, 1997, **244**, 45–58.
19 A. Cavallo, M. Müller and K. Binder, *Macromolecules*, 2006, **39**, 9539–9550.
20 S. Marrink, D. Tieleman and A. Mark, *J. Phys. Chem. B*, 2000, **104**, 12165–12173.
21 M. Jorge, *Langmuir*, 2008, **24**, 5714–5725.
22 S. Abel, J. Attia, S. Rémita, M. Marchi, W. Urbach and M. Goldmann, *Chem. Phys. Lett.*, 2009, **481**, 124–129.
23 M. Sammalkorpi, M. Karttunen and M. Haataja, *J. Phys. Chem. B*, 2007, **111**, 11722–11733.
24 M. Sammalkorpi, M. Karttunen and M. Haataja, *J. Phys. Chem. B*, 2009, **113**, 5863–5870.
25 M. Sammalkorpi, S. Sanders, A. Panagiotopoulos, M. Karttunen and M. Haataja, *J. Phys. Chem. B*, 2011, **115**, 1403–1410.
26 N. Hassan, J. Ruso and A. Piñeiro, *Langmuir*, 2011, **27**, 9719–9728.
27 S. A. Sanders, M. Sammalkorpi and A. Z. Panagiotopoulos, *J. Phys. Chem. B*, 2012, **116**, 2430–2437.
28 R. Braun, D. M. Engelman and K. Schulten, *Biophys. J.*, 2004, **87**, 754–763.
29 P. J. Bond, J. M. Cuthbertson, S. S. Deol and M. S. P. Sansom, *J. Am. Chem. Soc.*, 2004, **126**, 15948–15949.
30 R. A. Böckmann and A. Caflisch, *Biophys. J.*, 2005, **88**, 3191–3204.
31 H. Kuhn, B. Breitzke and H. Rehage, *Colloid Polym. Sci.*, 1998, **276**, 824–832.
32 C. Bruce, M. Berkowitz, L. Perera and M. Forbes, *J. Phys. Chem. B*, 2002, **106**, 3788–3793.
33 N. Yoshii and S. Okazaki, *Chem. Phys. Lett.*, 2006, **425**, 58–61.
34 B. Shang, Z. Wang and R. Larson, *J. Phys. Chem. B*, 2008, **112**, 2888–2900.
35 C. M. Jäger, A. Hirsch, C. Böttcher and T. Clark, in *Proceedings of the International Beilstein Symposium on Functional Nanoscience*, Beilstein-Institut, Bozen, 2010, pp. 91–106.
36 A. She, H. Gang and B. Mu, *Adv. Biomed. Res.*, 2010, 284–287.
37 T. Wang, C. Chipot, X. Shao and W. Cai, *Langmuir*, 2011, **27**, 91–97.
38 F. Palazzesi, M. Calvaresi and F. Zerbetto, *Soft Matter*, 2011, **7**, 9148–9156.
39 S. Burov, N. Obrezkov, A. Vanin and E. Piotrovskaya, *Colloid J.*, 2008, **70**, 1–5.
40 G. Mohan and D. Kopelevich, *J. Chem. Phys.*, 2008, **128**, 044905.
41 S. Samanta, S. Bhattacharya and P. Maiti, *J. Phys. Chem. B*, 2009, **113**, 13545–13550.
42 E. Wallace and M. Sansom, *Nanotechnology*, 2009, **20**, 045101.
43 B. Bhargava and M. Klein, *Mol. Phys.*, 2009, **107**, 393–401.
44 R. Wu, M. Deng, B. Kong and X. Yang, *J. Phys. Chem. B*, 2009, **113**, 15010–15016.
45 S. Sanders and A. Panagiotopoulos, *J. Chem. Phys.*, 2010, **132**, 114902.
46 P. J. Bond and M. S. P. Sansom, *J. Am. Chem. Soc.*, 2006, **128**, 2697–2704.
47 M. McCullagh, T. Prytkova, S. Tonzani, N. Winter and G. Schatz, *J. Phys. Chem. B*, 2008, **112**, 10388–10398.
48 S. Jalili and M. Akhavan, *Colloids Surf., A*, 2009, **352**, 99–102.
49 A. Nevidimov and V. Razumov, *Mol. Phys.*, 2009, **107**, 2169–2180.
50 J. Michel, M. Orsi and J. Essex, *J. Phys. Chem. B*, 2008, **112**, 657–660.
51 A. Rzepiela, M. Louhivuori, C. Peter and S. Marrink, *Phys. Chem. Chem. Phys.*, 2011, **13**, 10437–10448.

52 W. Tschöp, K. Kremer, O. Hahn, J. Batoulis and T. Bürger, *Acta Polym.*, 1998, **49**, 75–79.
53 A. Heath, L. Kavraki and C. Clementi, *Proteins*, 2007, **68**, 646–661.
54 C. Peter and K. Kremer, *Soft Matter*, 2009, **5**, 4357–4366.
55 A. Rzepiela, L. Schäfer, N. Goga, H. Risselada, A. De Vries and S. Marrink, *J. Comput. Chem.*, 2010, **31**, 1333–1343.
56 P. Stansfeld and M. Sansom, *J. Chem. Theory Comput.*, 2011, **7**, 1157–1166.
57 P. Mendoza-Espinosa, A. Moreno, R. Castillo and J. Mas-Oliva, *Biochem. Biophys. Res. Commun.*, 2008, **365**, 8–15.
58 D. Van der Spoel, E. Lindahl, B. Hess, G. Groenhof, A. Mark and H. Berendsen, *J. Comput. Chem.*, 2005, **26**, 1701–1718.
59 http://www.gromacs.org/.
60 H. Berendsen, J. Postma, W. Van Gunsteren, A. Dinola and J. Haak, *J. Chem. Phys.*, 1984, **81**, 3684–3690.
61 http://www.rasmol.org/.
62 http://www.pymol.org/.
63 S. Marrink, H. Risselada, S. Yefimov, D. Tieleman and A. de Vries, *J. Phys. Chem. B*, 2007, **111**, 7812–7824.
64 R. Stafford, T. Fanni and E. Dennis, *Biochemistry*, 1989, **28**, 5113–5120.
65 O. Berger, O. Edholm and F. Jähnig, *Biophys. J.*, 1997, **72**, 2002–2013.
66 http://moose.bio.ucalgary.ca/.
67 J. F. Kraft, M. Vestergaard, B. Schiøtt and L. Thøgersen, *J. Chem. Theory Comput.*, 2012, **8**, 1556–1569.
68 S. O. Yesylevskyy, L. V. Schäfer, D. Sengupta and S. J. Marrink, *PLoS Comput. Biol.*, 2010, **6**, 1–17.
69 M. Orsi, D. Haubertin, W. Sanderson and J. Essex, *J. Phys. Chem. B*, 2008, **112**, 802–815.
70 D. Uhríková, P. Rybár, T. Hianik and P. Balgavý, *Chem. Phys. Lipids*, 2007, **145**, 97–105.
71 J. Nagle and S. Tristram-Nagle, *Biochim. Biophys. Acta*, 2000, **1469**, 159–195.
72 G. Vitiello, D. Ciccarelli, O. Ortona and G. D'Errico, *J. Colloid Interface Sci.*, 2009, **336**, 827–833.
73 B. J. Berne and R. Pecora, *Dynamic Light Scattering: with Applications to Chemistry, Biology, and Physics*, Dover, N.Y, 2000.
74 Malvern_Instruments, What is the hydrodynamic radius?, http://www.malvern.com/, 2006.
75 B. B. Weiner, What is particle size?, http://www.brookhaven instruments.com/, 2010.
76 J. Mattila, K. Sabatini and P. Kinnunen, *Biophys. J.*, 2007, **93**, 3105–3112.
77 P. Niemelä, M. Miettinen, L. Monticelli, H. Hammaren, P. Bjelkmar, T. Murtola, E. Lindahl and I. Vattulainen, *J. Am. Chem. Soc.*, 2010, **132**, 7574–7575.
78 P. Niemelä, S. Ollila, M. Hyvönen, M. Karttunen and I. Vattulainen, *PLoS Comput. Biol.*, 2007, **3**, 304–312.
79 S. Deol, P. Bond, C. Domene and M. Sansom, *Biophys. J.*, 2004, **87**, 3737–3749.
80 H. Hayashi, T. Yamanaka, M. Miyajima and T. Imae, *Chem. Lett.*, 1994, 2407–2410.
81 C. Rosetti and C. Pastorino, *J. Phys. Chem. B*, 2011, **115**, 1002–1013.
82 E. Jardón-Valadez, A. Bondar and D. Tobias, *Biophys. J.*, 2009, **96**, 2572–2576.
83 The positional interpolation/extrapolation mapping-back approach from the MARTINI force field to a number of atomistic force fields was implemented for lipid membranes as a web application (beta version available at http://smmb.usc.es/sugarpie/sugarpie.php).